


Enhancement of the Curie temperature in single-crystalline ferromagnetic LaCrGe_3 by electron irradiation-induced disorder

E. H. Krenkel,^{1,2} M. A. Tanatar^{1,2,*}, M. Kończykowski³, R. Grasset³, Lin-Lin Wang¹,
S. L. Bud'ko^{1,2}, P. C. Canfield^{1,2} and R. Prozorov^{1,2,†}

¹Ames National Laboratory, Ames, Iowa 50011, USA

²Department of Physics and Astronomy, Iowa State University, Ames, Iowa 50011, USA

³Laboratoire des Solides Irradiés, CEA/DRF/IRAMIS, École Polytechnique, CNRS, Institut Polytechnique de Paris, F-91128 Palaiseau, France

 (Received 7 May 2024; revised 27 June 2024; accepted 1 July 2024; published 22 July 2024)

LaCrGe_3 has attracted attention as a potential candidate for studies of quantum phase transitions in a ferromagnetic material. The application of pressure avoids a quantum critical point by developing a new magnetic phase. It was suggested that the disorder may provide an alternative route to a quantum critical point. We used low-temperature 2.5 MeV electron irradiation to induce relatively small amounts of pointlike disorder in single crystals of LaCrGe_3 . Irradiation leads to an increase of the resistivity at all temperatures with some deviation from the Matthiessen rule. Hall effect measurements show that electron irradiation does not cause any detectable change in the carrier density. Unexpectedly, the Curie temperature, T_{FM} , increases with the increase of disorder from approximately 90 K in pristine samples up to nearly 100 K in the heavily irradiated sample, with a tendency towards saturation at higher doses. This effect is observed both in resistivity and magnetization measurements. Although the mechanism of this effect is not entirely clear, we conclude that it cannot be caused by effective “doping” or “pressure” due to electron irradiation. We suggest that disorder-induced broadening of a sharp peak in the density of states, $D(E)$, situated at $E_p = E_F - 0.25$ eV below the Fermi energy, E_F , causes an increase in $D(E_F)$, leading to an enhancement of T_{FM} in this itinerant ferromagnet.

DOI: [10.1103/PhysRevB.110.014429](https://doi.org/10.1103/PhysRevB.110.014429)

I. INTRODUCTION

Monotonic suppression of the transition temperature of second-order phase transitions to $T = 0$ by a nonthermal tuning parameter (pressure, composition, disorder, uniaxial strain, magnetic field) provides a fruitful playground for the realization of novel exotic phases of matter [1,2]. For example, quantum fluctuations of the antiferromagnetic order parameter on approaching a quantum critical point (QCP) lead to unconventional superconductivity in heavy fermion, cuprate, organic, and iron-based superconductors [3–5]. Fluctuations of the charge density wave (CDW) order parameter lead to an increase in superconducting T_c in $(\text{Ca}, \text{Sr})_3(\text{Rh}, \text{Ir})_4\text{Sn}_{13}$ compounds [6,7].

The application of similar ideas to ferromagnetic compounds has a fundamental problem. Quantum phase transitions in two-dimensional and three-dimensional metallic systems from a paramagnetic (PM) phase to a homogeneous ferromagnetic (FM) phase are generically first order, provided the material is sufficiently clean [8]. This is determined by the interaction of the magnetization with the electronic soft modes that exist in any metal, leading to a fluctuation-induced first-order transition. The exceptions are noncentrosymmetric metals with strong spin-orbit coupling [9]. As a result,

when tuning material to QCP, the continuous FM-PM transition either becomes an abrupt first-order transition below a tricritical point or modulated magnetic phases appear; see Refs. [10,11] for reviews. However, it has also been shown that nonmagnetic quenched disorder suppresses the tricritical temperature and the transition can remain second order down to zero temperature if the disorder strength exceeds a certain critical value, which opens new opportunities in studies of quantum criticality in small magnetic moment (fragile) ferromagnets [2,8]. This suggests that disorder may play a pivotal role in quantum critical behavior of ferromagnets.

One of the potentially strong effects of pointlike nonmagnetic disorder is its impact on the energy distribution of the density of states (DOS), $D(E)$. The ferromagnetic instability in a metal occurs when the Stoner criterion $ID(E_F) > 1$ is satisfied, where I is the Stoner parameter of the strength of the Coulomb interaction. Normally, random pointlike disorder leads to smearing of $D(E)$ causing a reduction of $D(E_F)$, thus destabilizing itinerant magnetism. However, if there is a peak in $D(E)$ not far from E_F , this smearing may cause an increase in $D(E_F)$ and enhance T_{FM} .

Substitutional disorder is an unavoidable component of systems in which composition variation is used as a tuning parameter, and disentangling its role from chemical doping/steric effects is very hard and sometimes impossible. Irradiation with energetic particles provides an alternative way to control the disorder. The use of disorder as a nonthermal tuning parameter, as, for example, in the cases of NbSe_2 [12]

*Contact author: tanatar@ameslab.gov

†Contact author: prozorov@ameslab.gov

and $(\text{Ba, K})\text{Fe}_2\text{As}_2$ [13,14], might provide a way to smear a first-order transition and enable a ferromagnetic quantum critical point [10,11].

LaCrGe_3 is a typical example of avoided quantum criticality in a ferromagnetic system. Upon the application of hydrostatic pressure, the Curie temperature (T_{FM}) is initially suppressed, but then the nature of the transition changes to the first order and a new magnetic phase is stabilized [15,16]. When the magnetic transition becomes first order at the tricritical point, application of a magnetic field H along the magnetization axis reveals a wing structure phase diagram in the T - p - H space, indicating the possibility of a new type of field-induced quantum critical point [17].

Motivated by the idea of using disorder as a tuning parameter to reveal quantum criticality in itinerant metallic ferromagnets, we present a study of the effects of a controlled disorder on magnetic ordering in LaCrGe_3 . Disorder was introduced by low temperature electron irradiation, creating defects in form of vacancies with densities on the order of 10^{-3} defects per atom (i.e., comparable to the disorder associated with one out of 200 unit cells having a defect). Contrary to theoretical predictions and general intuition, we found that the transition temperature to a ferromagnetic state in LaCrGe_3 is enhanced by the disorder. The effect is most likely caused by the specifics of the electronic band structure of this material, which shows a strong peak in the density of states below E_F .

II. METHODS

A. Samples

Unlike initial growths of this material [18], the single crystals of LaCrGe_3 used in this study were grown in two steps [19] from melts of $\text{La}_{18}\text{Cr}_{12}\text{Ge}_{70}$ [20,21] using fritted Canfield crucible sets (CCS) [22,23]. First $\text{La}_{18}\text{Cr}_{12}\text{Ge}_{70}$ was heated to 1150°C and cooled to 950°C over 50–100 h. At 950°C , a mixture of LaGe_{2-x} plates and LaCrGe_3 rods was separated from the remaining liquid phase. Subsequently, this decanted liquid was resealed, heated to 1000°C to fully remelt it, and then slowly cooled from 950°C to 825°C over roughly 100 h. At 825°C the growth was decanted and the resulting single phase LaCrGe_3 crystalline solid phase was separated from excess liquid.

Samples from the same batches used in our electron irradiation study were characterized by x-ray diffraction, resistance, and magnetization. The results were consistent with previous reports [16–18] in terms of the ferromagnetic Curie temperature (T_{FM}) and residual resistivity ratio (RRR); see Fig. 1 below.

B. Electrical transport

The rod-shaped single crystals with hexagonal cross sections were characterized by electrical resistivity and Hall effect measurements, with the electrical current along the long dimension of the sample corresponding to the c axis. Contacts to the samples were soldered in a standard four-probe resistivity measurement configuration and five-probe Hall effect configuration with indium. Conducting Dupont 4929N silver paste was used to mechanically stabilize the contacts [24].

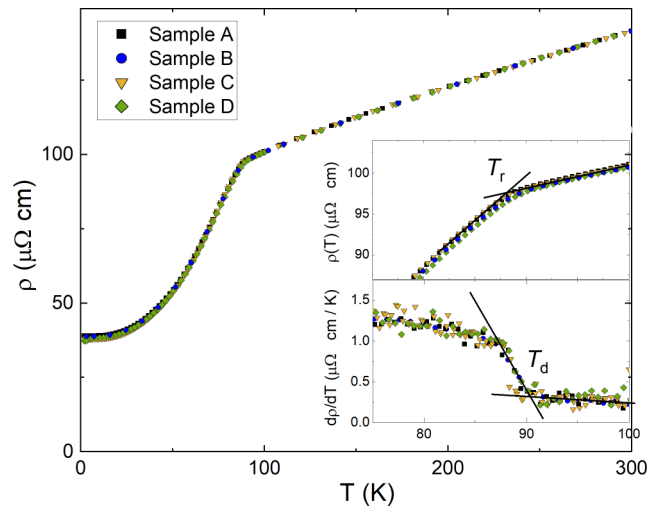


FIG. 1. Temperature dependent resistivity of the four selected samples of LaCrGe_3 . The room-temperature resistivity of LaCrGe_3 for the current along c axis was normalized to $141 \mu\Omega \text{ cm}$, a value obtained from an array of 11 samples. The geometric factors of all samples were adjusted to match this value. Insets zoom in on the transition temperature in resistivity (top inset) and the temperature derivative of the resistivity (bottom inset). The two criteria used for the determination of the transition temperatures from resistivity data, T_r , and from the onset of the derivative increase, T_d , are shown.

The typical contact resistance was in the 10 to 100 m Ω range. Temperature-dependent resistivity and Hall effect measurements were performed using a *Quantum Design* physical property measurement system (PPMS). The magnetic field for Hall effect measurements was applied along the a axis, transverse to the current flowing along the c axis.

Resistivity measurements at 300 K were performed on 11 samples of LaCrGe_3 with current along the c axis. Two samples were discarded as obvious outliers, and from the remainder the resistivity at room temperature was determined as $141 \pm 12 \mu\Omega \text{ cm}$. In the remainder of this paper, we use this value for all pristine c axis transport samples, and normalize geometric factors to match this value. For the irradiation study, we selected four samples, shown in Fig. 1, with highly reproducible temperature-dependent resistivity curves that lay on top of each other and are indistinguishable to the eye.

C. Magnetization

Magnetization was measured using a Quantum Design vibrating sample magnetometer (VSM) on a 9 T physical property measurement system (PPMS). The sample was fixed on a quartz sample holder with the magnetic field aligned along the long dimension of the sample corresponding to the c axis. The same sample B was measured in the pristine state and after the largest dose, 11 C/cm^2 , of electron irradiation.

D. Electron irradiation

Electron irradiation was performed at the “SIRIUS” Pelletron linear accelerator operated by Laboratoire des Solides Irradiés at École Polytechnique in Palaiseau, France [25]. The 2.5 MeV electrons impact the sample kept in liquid

TABLE I. Sample irradiation summary.

Sample	Thickness (μm)	Dose (C/cm^2)	Entry ($\text{dpa} \times 10^{-4}$)	Exit E (MeV)	Exit σ (barn)	Exit ($\text{dpa} \times 10^{-4}$)	Attenuation (%)	$\rho(300\text{ K})$, (% change) ($\mu\Omega\text{ cm}$)
A	133	3	21.3	2.27	105	19.7	92	150.0 (6%)
B	511	3	21.3	1.9	88	16.5	77	149 (5.6%)
C	222	0.5	3.55	2.17	101	3.15	89	142.0 (0.3%)
D	222	1	7.1	2.17	101	6.30	89	150.5 (7%)

hydrogen at 22 K to ensure efficient heat removal, and to prevent clustering and recombination of created atomic defects, vacancy and interstitial, called Frenkel pairs. Due to their small rest mass, the relativistic energy transfer upon impact from electrons matches the energy of ionic displacement barriers. Heavier particles and ions induce correlated disorder from secondary collisions and cascades, such as extended clusters and columnar defects. The typical threshold energy to displace the ions is between 10 and 100 eV [26–29].

The interstitials usually have lower diffusion barriers compared to vacancies. When the sample is returned to room temperature, some of the Frenkel pairs recombine, and some interstitials leave the crystal through various sinks, such as extended defects (dislocations/disclinations) and surfaces. The remaining metastable population of vacancies and interstitials is the point like disorder in our study [28,29]. The exact rate of annealing is material dependent and we use resistivity increase to quantify the added disorder.

The samples for resistivity measurements during and after electron irradiation were mounted on a thin mica plate, which was placed inside a hollow Kyocera chip C-QFN (ceramic quad flat nonleaded packages) [30]. The Kyocera chip, mounted on a special holder, was inserted into the irradiation chamber and kept in liquid hydrogen during irradiation.

For the analysis of the defect density we used an average cross section for LaCrGe_3 at 2.5 MeV, $\sigma = 114$ barn. This value gives 7.1×10^{-4} defects per atom per 1 C/cm^2 . While the incoming electron beam energy is at 2.5 MeV, the energy is gradually lost and in a sample of LaCrGe_3 it should go to zero at the thickness of 1.3 mm (stopping distance). This limits the practical acceptable thicknesses of the samples to 0.5 mm or less. In Table I we summarize parameters for the first irradiation run involving all the samples used in this study. For the thickest sample B the energy of the beam at the sample exit is calculated as 1.9 MeV. This energy is still sufficient to knock out all species of ions in the lattice [28,29]. Direct evidence for this conclusion comes from the identical increase of T_{FM} and resistivity shift in samples A (0.133 mm thick) and B (0.511 mm thick) after receiving an identical dose of irradiation; see Figs. 2, 3, and 5 below.

The flux of electrons was estimated by measuring the total electrical current through a 5 mm diameter diaphragm using a Faraday cup positioned behind the sample, so that only transmitted electrons were counted. The dose of electron irradiation received by a sample is reported in C/cm^2 . In conventional units, $1\text{ C}/\text{cm}^2 = 6.24 \times 10^{18}$ electrons/ cm^2 . Typically, the dose accumulated in a session varies from 0.5 (overnight) to 3 C/cm^2 (weekend). Larger doses are accumulated in several irradiation sessions, which can be separated by 6 to 12 months with *ex situ* sample characterization in

between. Since the density of defects produced by irradiation is metastable, some annealing occurs at room temperature between runs. Throughout the paper we use “pristine” and “unirradiated” interchangeably to describe samples that have not been exposed to electron irradiation. The doses shown in figures involving sample B are cumulative: 3 C/cm^2 from the first irradiation is listed as 3 C/cm^2 . When the same sample receives a second irradiation of 3 C/cm^2 , it is shown in the figure as 6 C/cm^2 (for the total dose), and so on. The initial doses for all samples are listed in column 2 of Table I.

E. Electronic band structure calculations

Density functional theory (DFT) with the local density approximation (LDA) as the exchange-correlation functional was used to relax structures and calculate the density of states (DOS) for LaCrGe_3 without and with vacancies. The DFT calculations were done using the Vienna Ab-initio Simulation Package (VASP) using projected augmented wave method and a plane-wave basis set with a kinetic energy cutoff of 227.2 eV. The primitive unit cell is fully relaxed on a $(7 \times 7 \times 8)$ Monkhorst-Pack k -point mesh including the Γ point with a Gaussian smearing of 0.05 eV and an increased kinetic energy cutoff of 1.25 times. The calculated lattice constants of 6.088 and 5.591 Å agree with the previously

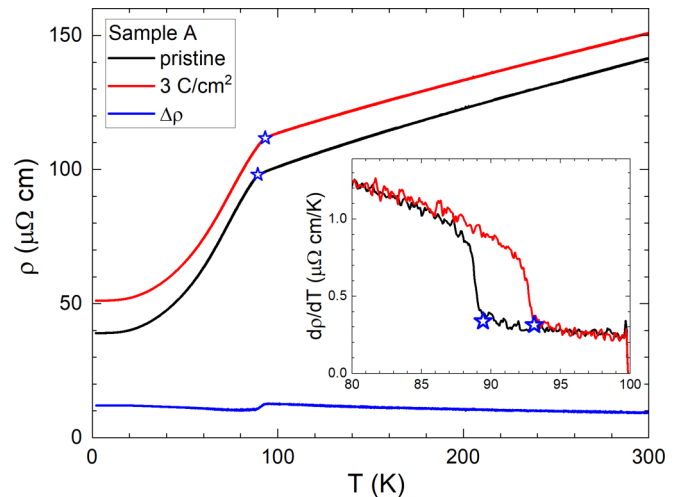


FIG. 2. Temperature-dependent resistivity of sample A before and after 3 C/cm^2 of electron irradiation. Stars mark the ferromagnetic transition temperature before and after irradiation using the T_f criterion. The inset shows the derivative of resistivity with respect to temperature, with stars defining the transition temperature using the T_d criterion. The blue line in the main panel shows the difference between resistivity curves before and after irradiation.

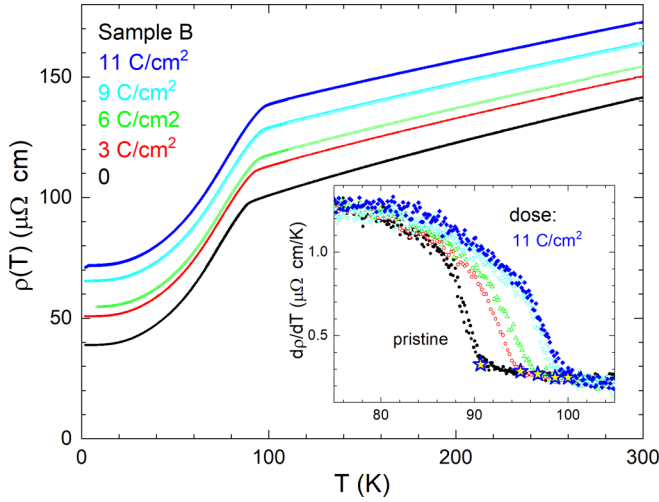


FIG. 3. Evolution of the temperature dependent longitudinal resistivity of sample B with sequential electron irradiations. The inset shows the derivative of the resistivity with respect to temperature. Resistivity shows nearly parallel upshift with irradiation dose.

calculated 6.078 and 5.587 Å [31], which are slightly underestimated when compared to the experimental data of 6.165 and 5.748 Å. For the accurate DOS calculation, a much denser ($12 \times 12 \times 18$) k -point mesh with the tetrahedron method is used. The ($3 \times 3 \times 3$) supercell with vacancies is relaxed on a ($2 \times 2 \times 3$) k -point mesh and the corresponding DOS calculated on a denser ($4 \times 4 \times 6$) k -point mesh. The absolute forces on ions are reduced to below 0.02 eV/Å during relaxation. Previous DFT calculations have shown that LDA with the fully relaxed crystal structure can give a total magnetic moment of $1.09 \mu_B$ – $1.12 \mu_B$ in a good agreement to the experimental data of $1.22 \mu_B$ – $1.25 \mu_B$ [18,19,31]. Our calculated $1.14 \mu_B$ with LDA also agrees with these results.

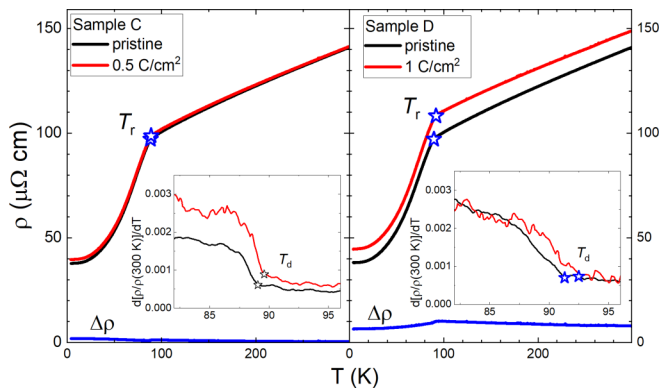


FIG. 4. Temperature-dependent resistivity of samples C (left panel) and D (right panel) before (black curves) and after (red curves) electron irradiation. Stars mark the ferromagnetic transition temperature before and after irradiation using T_r criterion. Insets show the derivative of resistivity with respect to temperature, with stars defining the transition temperatures using T_d criterion. Blue lines show the difference, $\Delta\rho = \rho(\text{irradiated}) - \rho(\text{pristine})$.

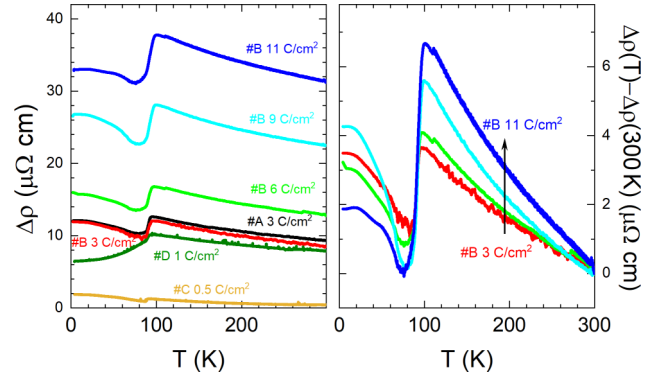


FIG. 5. Left panel: Shift of the temperature dependent resistivity, $\Delta\rho(T, \text{Dose}) = \rho(T, \text{Dose}) - \rho(T, 0\text{C/cm}^2)$. Sample A, after a dose of 3 C/cm² (black); sample B after multiple irradiations with cumulative doses of 3 C/cm² (red), 6 C/cm² (light green), 9 C/cm² (cyan), and 11 C/cm² (dark blue); sample C after 0.5 C/cm² (yellow); and sample D after 1 C/cm² (dark green) irradiation. The right panel shows the relative shifts in resistivity with respect to their values at room temperature, $\Delta\rho(T) - \Delta\rho(300\text{K})$.

III. RESULTS

We begin by comparing the impact of irradiation on different samples. Figure 1 shows the temperature-dependent resistivity of four crystals of LaCrGe₃. The inset zooms on the area close to T_{FM} in resistivity (top) and the temperature-dependent resistivity derivative (bottom). The selected samples show good reproducibility of both T_{FM} and RRR, as well as the overall temperature dependence of the resistivity. Insets also show two ways of the transition temperature determination. The crossing points of the linear fits of the $\rho(T)$ curves above and below the transition was used to determine T_r (upper inset). Similar linear fits of the derivative curves (lower inset) were used to define T_d .

Figure 2 shows the temperature-dependent resistivity of sample A before (black curve) and after 3 C/cm² of irradiation (red curve). The $\rho(T)$ curve demonstrates a nearly parallel shift with irradiation. The difference, $\Delta\rho(T) = \rho(T, 3\text{C/cm}^2) - \rho(T, \text{pristine})$ (blue line, main panel), shows minor violation of Matthiessen's rule, increasing from 9.5 $\mu\Omega\text{cm}$ at 300 K to 12.5 $\mu\Omega\text{cm}$ at 95 K, just above T_N . Below the transition, $\Delta\rho$ drops to 10.5 $\mu\Omega\text{cm}$ and increases on further cooling to 10 K to 12 $\mu\Omega\text{cm}$, saturating at this value.

Importantly, T_{FM} increases with irradiation, from 89.9 to 92.9 K using T_r criterion and from 90.6 to 94.9 K using T_d criterion, as shown in inset of Fig. 2. Because of the transition temperature increase, there is a notable feature in the difference plot at T_{FM} .

Figure 3 shows the longitudinal resistivity of the sample B in zero magnetic field (also used for Hall measurements) in the pristine state (black curve) and after multiple irradiations with cumulative doses of 3 C/cm² (red), 6 C/cm² (green, second irradiation of 3 C/cm² sample), 9 C/cm² (cyan, added 3 C/cm² to 6 C/cm²) and 11 C/cm² (blue, added 2 C/cm² to 9 C/cm² sample). The irradiation for the 9 and 11 C/cm² doses was applied approximately 6 months after the previous doses, while the 6 C/cm² dose was applied one year after the

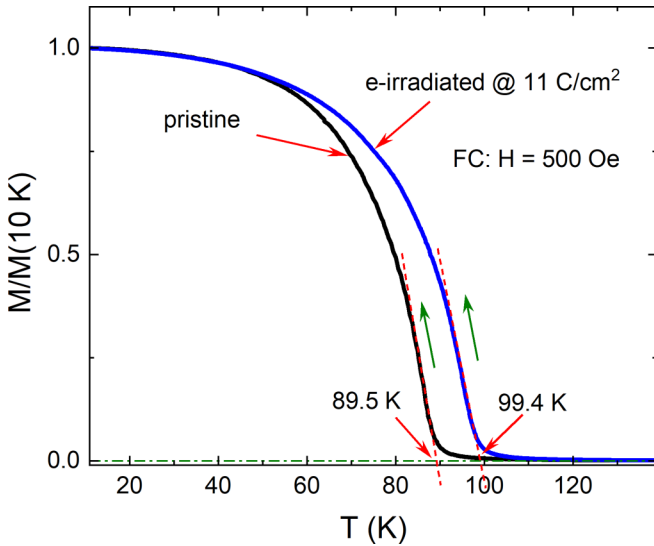


FIG. 6. Comparison of the temperature-dependent normalized magnetization, $M(T)/M(10\text{ K})$, measured on cooling (FC) in an applied magnetic field of 500 Oe in sample B before (red line) and after (blue line) 11 C/cm^2 electron irradiation. The definitions of the ferromagnetic transition temperatures are shown by stars.

sample initially received 3 C/cm^2 . This explains the visibly smaller shift between the 3 and 6 C/cm^2 curves compared to the other doses, due to longer time for partial annealing of the sample at room temperature [26,27]. Samples C and D were subjected to significantly smaller doses of irradiation (0.5 and 1 C/cm^2 respectively) and are shown in Fig. 4. Sample C followed the same trend in the transition temperature and resistivity with irradiation as samples A and B. Sample D showed a larger increase in both resistivity and the transition temperature per dose than the rest.

The temperature-dependent shift, $\Delta\rho$, for all samples is compared in Fig. 5. It has the same shape for samples A, B, and C, showing slight increase on cooling except for in the transition area.

Next, we examine the influence of electron irradiation on magnetization. Figure 6 shows the field-cooled (FC) normalized magnetization, $M/M(10\text{ K})$, in a magnetic field of 500 Oe measured in sample B in a pristine state (red line), and after the final dose of 11 C/cm^2 (blue line). This magnetic field was chosen to make sure there is no effect of magnetic domains that significantly influence the $M(T)$ curve. The transition temperature, T_M , increases from 89.5 K in the pristine state to 99.4 K, which agrees well with the temperature T_R from the resistivity measurements of the same sample B; see Fig. 3. The definitions of the magnetic transition temperature from $M(T)$ curves are shown in Fig. 6 by red dashed lines.

The shift in the resistivity at 300 K is a reasonable proxy for defect concentration. The bottom panel of Fig. 7 presents the variation of resistivity at $\rho(300\text{ K})$ as a function of irradiation dose. The top panel presents dose dependence of the ferromagnetic transition temperatures determined from resistivity using T_r (closed symbols) and T_d (open symbols) criteria. Stars show the results from $M(T)$. The dependence of the ferromagnetic transition temperature on $\rho(300\text{ K})$ is

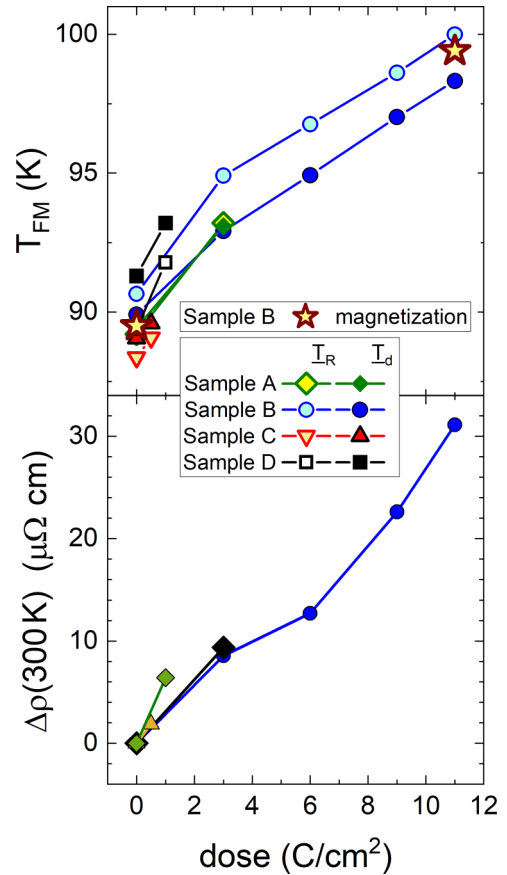


FIG. 7. Top panel: Dose dependence of ferromagnetic Curie temperature T_{FM} determined from resistivity measurements using T_r (closed symbols) and T_d (open symbols) criteria. Stars show the results from magnetization, Fig. 6. Bottom panel: Dose dependence of the shift of the room temperature resistivity, $\Delta\rho(300\text{ K, Dose}) = \rho(300\text{ K, Dose}) - \rho(300\text{ K, 0})$.

shown in Fig. 8. It is clear that, despite some variation of T_{FM} in the pristine state, all samples show a consistent trend of T_{FM} increase with increased disorder. When sample B was

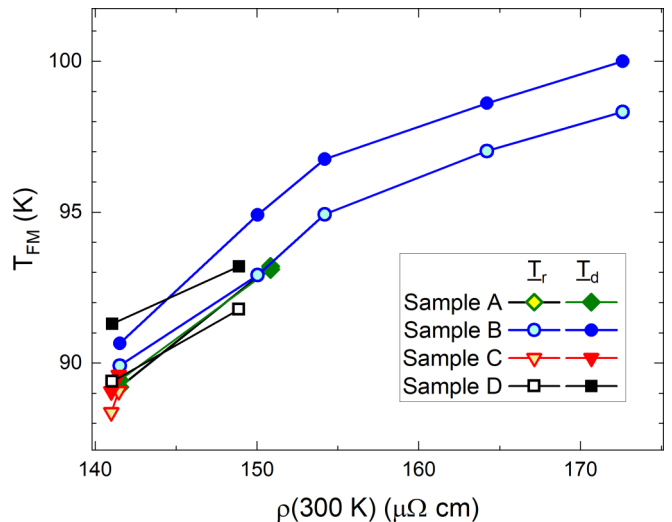


FIG. 8. Change in the ferromagnetic transition temperature in single crystals of LaCrGe_3 as a function of the room temperature resistivity, which is used here as a proxy for the amount of disorder.

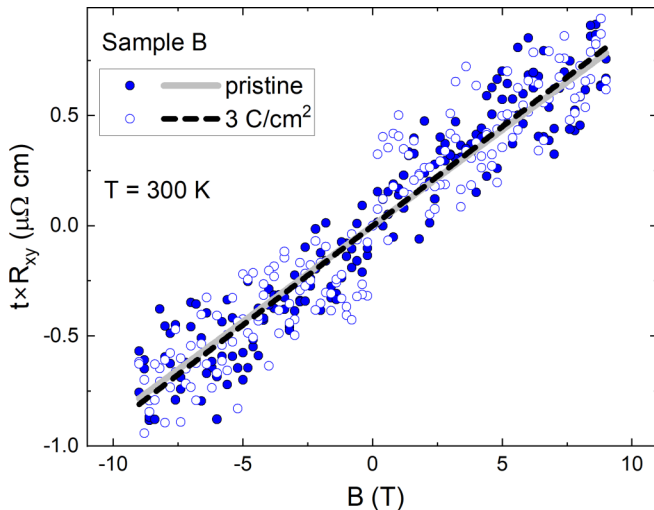


FIG. 9. A product of the transverse Hall resistance R_{xy} of sample B and its thickness t before and after irradiation as a function of magnetic field. Lines show the linear fit used for finding the Hall coefficient at 300 K. At this temperature, the difference in carrier density with irradiation is insignificant to within error ($9.0 \pm 0.2 \times 10^{-4}$ vs $8.7 \pm 0.2 \times 10^{-4}$ cm^3/C), showing that irradiation does not dope the system.

subjected to higher doses of irradiation, it revealed a trend toward $T_{\text{FM}}(\rho)$ saturation.

Finally, Fig. 9 presents field-dependent Hall resistance R_{xy} multiplied by sample thickness in sample B at room temperature, in the paramagnetic state far above the long range ordering at T_{FM} . The data in the pristine state are shown with solid symbols, and after $3 \text{ C}/\text{cm}^2$ electron irradiation with open symbols. Unfortunately, the contact for the transverse (Hall) resistance measurement deteriorated after $6 \text{ C}/\text{cm}^2$ of irradiation and mechanically detached after $9 \text{ C}/\text{cm}^2$. For both data sets the Hall resistance is linear in magnetic field, and have identical linear fit slopes (grey and dashed lines) to within error ($9.0 \pm 0.2 \times 10^{-4}$ to $8.7 \pm 0.2 \times 10^{-4}$ cm^3/C). This suggests that the change (increase) of the carrier density, if any, is less than 3%. This should be compared to the 6% change of resistivity for the same doses. The sign of the Hall effect is consistent with the sign of reported thermopower [32].

IV. DISCUSSION

Summarizing our observations, we see three effects of controlled disorder on the properties of LaCrGe_3 crystals. (1) The resistivity increases with disorder roughly independently of temperature and reveals only minor deviations from the Matthiessen's rule both above and below T_{FM} . These deviations diminish further with dose increase. (2) The resistivity increase is not accompanied by any sizable change of the Hall effect in the paramagnetic phase well above T_{FM} . This suggests that irradiation primarily changes the elastic scattering rate and is not changing the Fermi surface. (3) The ferromagnetic transition temperature, T_{FM} , is increased nearly linearly as a function of dose for small amounts of irradiation in all samples studied. At high doses there is a tendency toward saturation.

Theoretically, for a general case of an itinerant system, an increase in disorder suppresses the ferromagnetic transition temperature, T_{FM} , due to the smearing of DOS leading to the reduction of $D(E_F)$. Is it possible that similar smearing could instead result in an increase of $D(E_F)$ in LaCrGe_3 ? The top panel in Fig. 10 plots the band structure of the pristine ferromagnetic LaCrGe_3 showing the almost-flat bands at $E_F - 0.25 \text{ eV}$ for spin majority in a good agreement with the previous DFT study [31]. Then the bottom panel presents DOS in LaCrGe_3 calculated for the pristine structure and for the structure with 1.8% vacancies, the lowest concentration of vacancies suitable for a $(3 \times 3 \times 3)$ supercell, as shown in the middle panel. The average distance among these vacancy sites is about 8 \AA . The vacancy sites are separated among themselves by at least a full unit cell in all directions. The characteristic feature of band structure of LaCrGe_3 is a sharp peak in $D(E)$ located near $E_F - 0.25 \text{ eV}$ (black line) [31] originating from the almost flat Cr $3d$ bands (d_{xz} and d_{yz} orbitals) in the spin majority along the Γ - M - K - Γ direction. Noticeably DOS right at E_F for spin majority is very small and even smaller than that of the spin minority. Vacancies induce disorder by disrupting chemical bonds. As shown in the bottom panel of Fig. 10, 1.8% vacancies notably reduce and broaden the peak near $E_F - 0.25 \text{ eV}$ (red line). However, as the consequence of the broadening, the DOS at E_F shows a sizable increase for the majority spin, while it slightly decreases for the minority spin. Such opposite changes in the DOS at E_F vs $E_F - 0.25 \text{ eV}$ are also true with ionic relaxation (blue line). The overall DOS at E_F increases by 0.5 states/f.u. or 25%, accounting for both spin channels. The broadening of almost-flat bands at $E_F - 0.25 \text{ eV}$ leads to an increase of the DOS at E_F .

The calculated significant increase of DOS for a sample with 1.8% vacancies, should be scaled down to match the significantly lower densities of the vacancies introduced by irradiation in our experiments. As we have shown, the actual density is about one order of magnitude smaller for the highest doses achieved. Although an increase in $D(E_F)$ provides a plausible mechanism for T_c increase, it should lead to a slope change of resistivity curve due to carrier density variation, violation of Matthiessen's rule and a change in the Hall effect. Neither is obvious in our experiment, which may suggest that the states from the broadened flat bands remain localized.

Suppression of the ordering transition temperature with disorder is a general trend for materials with different types of order. Examples include a nematic/antiferromagnetic transition in the parent iron-based superconductor BaFe_2As_2 , isoelectron substituted $\text{BaFe}_2(\text{As}_{1-x}\text{P}_x)_2$ [33], and in hole-doped $(\text{Ba}_{1-x}\text{K}_x)\text{Fe}_2\text{As}_2$ [34]. Similar suppression of the charge density wave transition temperature with disorder is found in NbSe_2 [12,35], TaSe_2 , and TaS_2 [35,36]. Disorder suppresses the transition temperature in nodal superconductors [37], but the T_c is practically insensitive to disorder in conventional s -wave superconductors (known as the Anderson theorem) [38], with the exceptions coming from the effect of strong disorder on the density of states as observed in aluminum [39].

The exceptions to this common trend of ordering temperature suppression are mostly found in systems with competing orders. For example, in NbSe_2 [12,35], TaSe_2 [35],

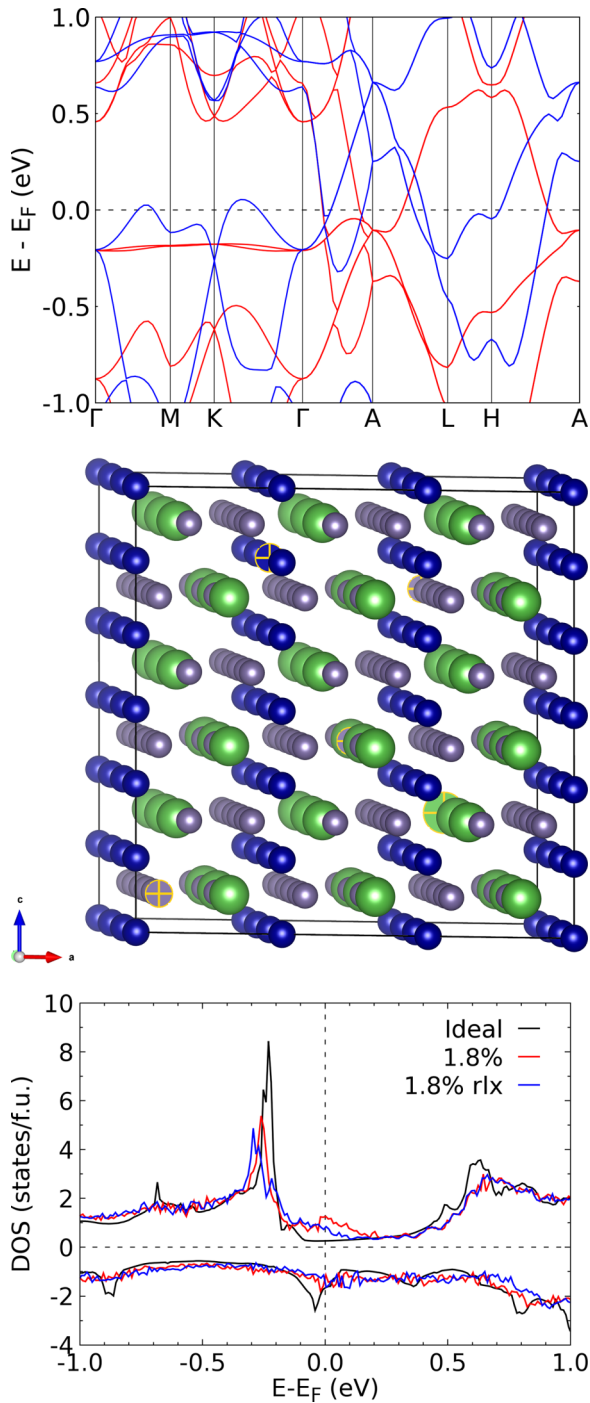


FIG. 10. Top panel: electronic band structure of pristine ferromagnetic LaCrGe_3 with spin majority in red and minority in blue. Middle panel: the supercell structure of LaCrGe_3 with La, Cr, and Ge ions shown by green, blue, and grey spheres, respectively. One formula unit (i.e., one La, one Cr, and three Ge atoms labeled with yellow crosses) are removed to create vacancies of 1.8% to represent disorder. Bottom panel: the density of states, $D(E)$, of ferromagnetic LaCrGe_3 in pristine state (black line) and in a $(3 \times 3 \times 3)$ supercell with 1.8% vacancies, as shown in the top panel. The red line is calculation with the rigid structure, the blue line is calculation after ionic relaxation. The spin majority (minority) DOS is plotted as positive (negative) value. The sharp DOS peak in the pristine state near $E_F - 0.25$ eV is broadened by vacancies and leads to a notable increase in the DOS at E_F .

TaS_2 [35,36], $\text{Lu}_5\text{Ir}_4\text{Si}_{20}$ [40], cuprates [41] and some Re-meika 3-4-13 compounds [42] superconducting T_c increases on suppression of CDW. In all these materials two electronic orders are competing for the density of states at the Fermi surface, and disorder tips the balance in favor of subdominant order (superconductivity) by suppressing dominant (higher transition temperature) order [43]. Similar phenomena are observed in FeSe , in which superconductivity is competing with nematic order [44]. The only exception to this rule is observed in $(\text{Ba}_{1-x}\text{K}_x)\text{Fe}_2\text{As}_2$, where dominant C_2 stripe antiferromagnetic order is stabilized when the subdominant (lower transition temperature) C_4 phase is suppressed by disorder [13]. The possibility of competing phases in LaCrGe_3 is suggested by the observation of several types of ordering in the pressure phase diagram [15]. Another ferromagnetic phase was suggested to be stabilized in LaCrGe_3 at ambient pressure below ~ 70 K [19,45].

Another mechanism that could potentially explain the observed change in T_{FM} would be an effective change in the average volume of the unit cell due to induced atomic defects. Experiments on neutron-irradiated Cu [46], electron-irradiated Cu [47], and electron-irradiated Al [48] showed that the lattice expands at low temperature, which is equivalent to a “negative effective pressure.” When measurements were performed as a function of temperature, it was found that at room temperature about 16% of the effective lattice parameter change at low temperatures, $\Delta a/a$, remained in copper and no resolvable leftover strain was observed in aluminum. The annealing process has several stages and is quite complicated. In this scenario, the effect of irradiation would result in an effective shrinkage of the lattice, exerting “positive effective pressure.” Therefore, the sign of the effect depends on the material and conditions of irradiation and thermal history of the sample.

Regardless the sign, let us estimate the volume change due to defects produced by irradiation, which will allow comparison with studies of LaCrGe_3 under pressure. One way is to estimate the total volume of all vacancies, assuming that no interstitials are left. Irradiation with the dose of 1 C/cm^2 induces about 3.5×10^{-3} vacancies per conventional unit cell, which is approximately 0.005 \AA^3 . With a unit cell volume of 218.5 \AA^3 , this gives $\Delta V/V \approx 2.2 \times 10^{-5}$ change. Our highest irradiation dose was 11 C/cm^2 , see Fig. 3, which results in $\Delta V/V \approx 2.5 \times 10^{-4}$ total volume change. On the opposite side of the estimate, we can assume that all defects stay and result in a rate of change reported for Cu and Al in Ref. [47]. Remarkably, it was found that at low temperatures the rate of change, $\eta = (\Delta V/V)/\Delta\rho$, does not vary much for a wide range of irradiation conditions [46–48]. For example, for copper irradiated with 2.6 MeV electrons at 6 K (quite similar to the parameters of our work), $\eta = 1.75 (\mu\Omega \text{ cm})^{-1}$ was reported [47]. As shown in Fig. 3, 11 C/cm^2 results in a resistivity change of $\Delta\rho \approx 38 \mu\Omega \text{ cm}$. This gives $\Delta V/V \approx 4.4 \times 10^{-4}$ total volume change, which is of the same order as the first estimate. However, the reported change of resistivity in the LaCrGe_3 was measured after the irradiated sample was brought up to the room temperature. According to Ref. [47] only about 16% of the effect remains for the linear change of the lattice parameter $\Delta a/a$. Therefore, the estimate becomes $\Delta V/V \approx 3.5 \times 10^{-6}$ for the

total volume change, which is much smaller than the first estimate.

In our experiments, the enhancement of T_{FM} per 1 C/cm² dose of electron irradiation is about 0.6 K. From the pressure dependence studies, this change is achieved at approximately 0.04 GPa. With a bulk modulus of 88 GPa (Ref. [45] in Ref. [49]), this corresponds to $\Delta V/V \approx 4.5 \times 10^{-4}$. This is $4.5 \times 10^{-4}/2.2 \times 10^{-5} \approx 20.5$ times larger than our largest estimate for the effect of irradiation for 1 C/cm². With the effect of annealing, this is 130 times larger than the realistic volume change due to defect formation by electron irradiation. Therefore, steric effects are unlikely to be the reason for the disorder-induced enhancement of the transition temperature.

V. CONCLUSION

In conclusion, we observed an enhancement of the ferromagnetic transition temperature in LaCrGe₃ with the

increasing concentration of pointlike defects. This contradicts theoretical predictions of the suppression of itinerant ferromagnetism by disorder [10,11]. We suggest that the flat band peak in $D(E)$ 0.25 eV below the E_F broadens with disorder, causing an apparent increase in $D(E_F)$ which leads to an increase of T_{FM} in this itinerant system.

ACKNOWLEDGMENTS

The research was supported by the U.S. Department of Energy, Office of Basic Energy Sciences, Division of Materials Sciences and Engineering. Ames National Laboratory is operated for the U.S. Department of Energy by Iowa State University under Contract No. DE-AC02-07CH11358. The authors acknowledge support from the EMIRA French network (FR CNRS 3618) on the SIRIUS platform under Project No. 21-3700.

-
- [1] B. Keimer, S. A. Kivelson, M. R. Norman, S. Uchida, and J. Zaanen, From quantum matter to high-temperature superconductivity in copper oxides, *Nature (London)* **518**, 179 (2015).
- [2] P. C. Canfield and S. L. Bud'ko, Preserved entropy and fragile magnetism, *Rep. Prog. Phys.* **79**, 084506 (2016).
- [3] N. D. Mathur, F. M. Grosche, S. R. Julian, I. R. Walker, D. M. Freye, R. K. W. Haselwimmer, and G. G. Lonzarich, Magnetically mediated superconductivity in heavy fermion compounds, *Nature (London)* **394**, 39 (1998).
- [4] L. Taillefer, Scattering and pairing in cuprate superconductors, *Annu. Rev. Condens. Matter Phys.* **1**, 51 (2010).
- [5] S. Kasahara, T. Shibauchi, K. Hashimoto, K. Ikada, S. Tonegawa, R. Okazaki, H. Shishido, H. Ikeda, H. Takeya, K. Hirata, T. Terashima, and Y. Matsuda, Evolution from non-Fermi- to Fermi-liquid transport via isovalent doping in BaFe₂(As_{1-x}P_x)₂ superconductors, *Phys. Rev. B* **81**, 184519 (2010).
- [6] L. E. Klintberg, S. K. Goh, P. L. Alireza, P. J. Saines, D. A. Tompsett, P. W. Logg, J. Yang, B. Chen, K. Yoshimura, and F. M. Grosche, Pressure- and composition-induced structural quantum phase transition in the cubic superconductor (Sr, Ca)₃Ir₄Sn₁₃, *Phys. Rev. Lett.* **109**, 237008 (2012).
- [7] S. K. Goh, D. A. Tompsett, P. J. Saines, H. C. Chang, T. Matsumoto, M. Imai, K. Yoshimura, and F. M. Grosche, Ambient pressure structural quantum critical point in the phase diagram of (Ca_xSr_{1-x})₃Rh₄Sn₁₃, *Phys. Rev. Lett.* **114**, 097002 (2015).
- [8] D. Belitz, T. R. Kirkpatrick, and T. Vojta, Nonanalytic behavior of the spin susceptibility in clean Fermi systems, *Phys. Rev. B* **55**, 9452 (1997).
- [9] T. R. Kirkpatrick and D. Belitz, Ferromagnetic quantum critical point in noncentrosymmetric systems, *Phys. Rev. Lett.* **124**, 147201 (2020).
- [10] D. Belitz, T. R. Kirkpatrick, and T. Vojta, How generic scale invariance influences phase transitions, *Rev. Mod. Phys.* **77**, 579 (2005).
- [11] M. Brando, D. Belitz, F. M. Grosche, and T. R. Kirkpatrick, Metallic quantum ferromagnets, *Rev. Mod. Phys.* **88**, 025006 (2016).
- [12] K. Cho, M. Kończykowski, S. Teknowijoyo, M. A. Tanatar, J. Guss, P. B. Gartin, J. M. Wilde, A. Kreyssig, R. J. McQueeney, A. I. Goldman, V. Mishra, P. J. Hirschfeld, and R. Prozorov, Using controlled disorder to probe the interplay between charge order and superconductivity in NbSe₂, *Nat. Commun.* **9**, 2796 (2018).
- [13] E. I. Timmons, M. A. Tanatar, K. Willa, S. Teknowijoyo, Kyuil Cho, M. Kończykowski, O. Cavani, Yong Liu, T. A. Lograsso, U. Welp, and R. Prozorov, Competition between orthorhombic and re-entrant tetragonal phases in underdoped Ba_{1-x}K_xFe₂As₂ probed by the response to controlled disorder, *Phys. Rev. B* **99**, 054518 (2019).
- [14] M. A. Tanatar, E. I. Timmons, M. Kończykowski, O. Cavani, K. Cho, Y. Liu, T. A. Lograsso, and R. Prozorov, Effect of controlled pointlike disorder induced by 2.5-MeV electron irradiation on the nematic resistivity anisotropy of hole-doped (Ba, K)Fe₂As₂, *Phys. Rev. B* **102**, 144511 (2020).
- [15] E. Gati, J. M. Wilde, R. Khasanov, L. Xiang, S. Dissanayake, R. Gupta, M. Matsuda, F. Ye, B. Haberl, U. Kaluarachchi, R. J. McQueeney, A. Kreyssig, S. L. Bud'ko, and P. C. Canfield, Formation of short-range magnetic order and avoided ferromagnetic quantum criticality in pressurized LaCrGe₃, *Phys. Rev. B* **103**, 075111 (2021).
- [16] V. Taufour, U. S. Kaluarachchi, R. Khasanov, M. C. Nguyen, Z. Guguchia, P. K. Biswas, P. Bonfà, R. De Renzi, X. Lin, Stella K. Kim, E. D. Mun, H. Kim, Y. Furukawa, C.-Z. Wang, K.-M. Ho, S. L. Bud'ko, and P. C. Canfield, Ferromagnetic quantum critical point avoided by the appearance of another magnetic phase in LaCrGe₃ under pressure, *Phys. Rev. Lett.* **117**, 037207 (2016).
- [17] U. S. Kaluarachchi, S. L. Bud'ko, P. C. Canfield, and V. Taufour, Tricritical wings and modulated magnetic phases in LaCrGe₃ under pressure, *Nat. Commun.* **8**, 546 (2017).
- [18] X. Lin, V. Taufour, S. L. Bud'ko, and P. C. Canfield, Suppression of ferromagnetism in the LaV_xCr_{1-x}Ge₃ system, *Phys. Rev. B* **88**, 094405 (2013).
- [19] M. Xu, S. L. Bud'ko, R. Prozorov, and P. C. Canfield, Unusual coercivity and zero-field stabilization of fully saturated

- magnetization in single crystals of LaCrGe_3 , *Phys. Rev. B* **107**, 134437 (2023).
- [20] P. C. Canfield, New materials physics, *Rep. Prog. Phys.* **83**, 016501 (2020).
- [21] T. J. Slade and P. C. Canfield, Use of refractory-volatile element deep eutectic regions to grow single crystalline intermetallic compounds, *Z. Anorg. Allg. Chem.* **648**, e202200145 (2022).
- [22] P. C. Canfield, T. Kong, U. S. Kaluarachchi, and N. H. Jo, Use of frit-disc crucibles for routine and exploratory solution growth of single crystalline samples, *Philos. Mag.* **96**, 84 (2016).
- [23] LSP Industrial Ceramics, Canfield crucible sets, <https://www.lspceramics.com/canfield-crucible-sets-2>, 2015.
- [24] M. A. Tanatar, A. E. Böhmer, E. I. Timmons, M. Schütt, G. Drachuck, V. Taufour, K. Kothapalli, A. Kreyssig, S. L. Bud'ko, P. C. Canfield, R. M. Fernandes, and R. Prozorov, Origin of the resistivity anisotropy in the nematic phase of FeSe , *Phys. Rev. Lett.* **117**, 127001 (2016).
- [25] Electron irradiation facility, <http://emir.in2p3.fr/LSI>.
- [26] K. Cho, M. Kończykowski, M. A. Tanatar, I. I. Mazin, Y. Liu, T. A. Lograsso, and R. Prozorov, Ion-selective scattering studied using the variable-energy electron irradiation in the $\text{Ba}_{0.2}\text{K}_{0.8}\text{Fe}_2\text{As}_2$ superconductor, *Materials* **16**, 4520 (2023).
- [27] K. Cho, M. Kończykowski, S. Teknowijoyo, M. A. Tanatar, and R. Prozorov, Using electron irradiation to probe iron-based superconductors, *Supercond. Sci. Technol.* **31**, 064002 (2018).
- [28] A. C. Damask and G. J. Dienes, *Point Defects in Metals* (Gordon & Breach, London, 1963).
- [29] M. W. Thompson, *Defects and Radiation Damage in Metals*, Cambridge Monographs on Physics (Cambridge University Press, Cambridge, 1969).
- [30] https://global.kyocera.com/prdct/semicon/semi/std_pkg/.
- [31] M. C. Nguyen, V. Taufour, S. L. Bud'ko, P. C. Canfield, V. P. Antropov, C.-Z. Wang, and K.-M. Ho, Using first-principles calculations to screen for fragile magnetism: Case study of LaCrGe_3 and LaCrSb_3 , *Phys. Rev. B* **97**, 184401 (2018).
- [32] D. Das, T. Gruner, H. Pfau, U. B. Paramanik, U. Burkhardt, C. Geibel, and Z. Hossain, Heavy fermion and Kondo lattice behavior in the itinerant ferromagnet CeCrGe_3 , *J. Phys.: Condens. Matter* **26**, 106001 (2014).
- [33] Y. Mizukami, M. Kończykowski, K. Matsuura, T. Watashige, S. Kasahara, Y. Matsuda, and T. Shibauchi, Impact of disorder on the superconducting phase diagram in $\text{BaFe}_2(\text{As}_{1-x}\text{P}_x)_2$, *J. Phys. Soc. Jpn.* **86**, 083706 (2017).
- [34] R. Prozorov, M. Kończykowski, M. A. Tanatar, H.-H. Wen, R. M. Fernandes, and P. C. Canfield, Interplay between superconductivity and itinerant magnetism in underdoped $\text{Ba}_{1-x}\text{K}_x\text{Fe}_2\text{As}_2$ ($x = 0.2$) probed by the response to controlled point-like disorder, *npj Quantum Mater.* **4**, 34 (2019).
- [35] H. Mutka, Superconductivity in irradiated charge-density-wave compounds 2H-NbSe_2 , 2H-TaS_2 , and 2H-TaSe_2 , *Phys. Rev. B* **28**, 2855 (1983).
- [36] L. Li, X. Deng, Z. Wang, Y. Liu, M. Abeykoon, E. Dooryhee, A. Tomic, Y. Huang, J. B. Warren, E. S. Bozin, S. J. L. Billinge, Y. Sun, Y. Zhu, G. Kotliar, and C. Petrovic, Superconducting order from disorder in $2\text{H-TaSe}_{2-x}\text{S}_x$, *npj Quantum Mater.* **2**, 11 (2017).
- [37] C. C. Tsuei and J. R. Kirtley, Pairing symmetry in cuprate superconductors, *Rev. Mod. Phys.* **72**, 969 (2000).
- [38] P. Anderson, Theory of dirty superconductors, *J. Phys. Chem. Solids* **11**, 26 (1959).
- [39] See, for example, R. W. Cohen and B. Abeles, Superconductivity in granular aluminum films, *Phys. Rev.* **168**, 444 (1968) and references therein.
- [40] M. Leroux, V. Mishra, C. Opagiste, P. Rodière, A. Kayani, W.-K. Kwok, and U. Welp, Charge density wave and superconductivity competition in $\text{Lu}_5\text{Ir}_4\text{Si}_{10}$: A proton irradiation study, *Phys. Rev. B* **102**, 094519 (2020).
- [41] M. Leroux, V. Mishra, J. P. C. Ruff, H. Claus, M. P. Smylie, C. Opagiste, P. Rodière, A. Kayani, G. D. Gu, J. M. Tranquada, W.-K. Kwok, Z. Islam, and U. Welp, Disorder raises the critical temperature of a cuprate superconductor, *Proc. Natl. Acad. Sci. USA* **116**, 10691 (2019).
- [42] E. H. Krenkel, M. A. Tanatar, M. Kończykowski, R. Grasset, E. I. Timmons, S. Ghimire, K. R. Joshi, Y. Lee, Liqin Ke, Shuzhang Chen, C. Petrovic, P. P. Orth, M. S. Scheurer, and R. Prozorov, Possible unconventional pairing in $(\text{Ca}, \text{Sr})_3(\text{Ir}, \text{Rh})_4\text{Sn}_{13}$ superconductors revealed by controlling disorder, *Phys. Rev. B* **105**, 094521 (2022).
- [43] A. M. Gabovich, A. I. Voitenko, and M. Ausloos, Charge- and spin-density waves in existing superconductors: competition between Cooper pairing and Peierls or excitonic instabilities, *Phys. Rep.* **367**, 583 (2002).
- [44] S. Teknowijoyo, K. Cho, M. A. Tanatar, J. Gonzales, A. E. Böhmer, O. Cavani, V. Mishra, P. J. Hirschfeld, S. L. Bud'ko, P. C. Canfield, and R. Prozorov, Enhancement of superconducting transition temperature by pointlike disorder and anisotropic energy gap in FeSe single crystals, *Phys. Rev. B* **94**, 064521 (2016).
- [45] R. R. Ullah, P. Klavins, X. D. Zhu, and V. Taufour, Magnetic domain depinning as possible evidence for two ferromagnetic phases in LaCrGe_3 , *Phys. Rev. B* **107**, 184431 (2023).
- [46] U. Himmler, H. Peisl, A. Sepp, W. Waidelich, H. Wenzl, Effect of annealing on the lattice parameter of neutron-irradiated copper, *Phys. Rev. Lett.* **19**, 956 (1967).
- [47] F. Dworschak, H. Wagner, and P. Wombacher, Comparison of lattice parameter and resistivity change in electron-irradiated copper, *Phys. Status Solidi B* **52**, 103 (1972).
- [48] H. Wagner, F. Dworschak, W. Schilling, Comparison of lattice-parameter and resistivity change in electron-irradiated aluminum, *Phys. Rev. B* **2**, 3856 (1970).
- [49] R. A. Ribeiro, S. L. Bud'ko, L. Xiang, D. H. Ryan, P. C. Canfield, Small-moment antiferromagnetic ordering in single-crystalline La_2Ni_7 , *Phys. Rev. B* **105**, 014412 (2022).